Fundamental properties of magnetized plasma flows

IEPC-2011-137

Presented at the 32nd International Electric Propulsion Conference,
Wiesbaden, Germany
September 11–15, 2011

T. Andreussi*
Alta S.p.A., Pisa, 56121, Italy

S. Giannelli†
University of Pisa, Pisa, 56122, Italy

F. Pegoraro‡
University of Pisa, Pisa, 56127, Italy

and

M. Andrenucci§
University of Pisa, Pisa, 56122, Italy
Alta S.p.A., Pisa, 56121, Italy

An axisymmetric, resistive magnetohydrodynamic description of steady-state plasma flows is introduced in order to analyse the plasma acceleration process inside self-field magnetoplasmadynamic (MPD) thrusters. Cylindrical and conical configurations of the acceleration channel are investigated by first neglecting the effects of the gasdynamic pressure. A special class of 2D poloidal solutions is introduced and a simple analytical description of the flow is obtained in terms of two characteristic parameters: the magnetic Reynolds number and a dimensionless parameter which depends on the applied voltage. The modifications induced by the gasdynamic effects are then considered, for the cylindrical configuration, by assuming a smooth sonic transition of the flow. The dependence of thrust efficiency on the characteristic parameters of the model is pointed out and the results obtained in previous investigations are recovered and generalized.

I. Introduction

Designers of future manned space missions, towards Mars and the outer planets, will face the need of a propulsion system able to offer sufficiently high values of thrust, in the order of 1 N or above, and yet offering medium to high values of specific impulse, in the order of a thousand seconds or above. The requirement on the thrust level is a direct consequence of the time requirements those mission are subject to in order to reduce the time astronauts will have to spend travelling, being exposed to harmful cosmic radiations. The requirement on the specific impulse is obviously a direct consequence of the mass-saving paradigm in space engineering, and yet the required I_{sp} must not be too high, in order to comply with onboard power limits, given the high thrust level.

The previously cited propulsion parameters should be fitted by Magnetoplasmadynamic (MPD) thrusters, both in the applied-field (AF-MPD) and self-field (SF-MPD) configurations, the first offering (in common

*Research Engineer, Alta S.p.A., t.andreussi@alta-space.com.
†Ph.D. Student, Aerospace Engineering Department, s.giannelli@alta-space.com.
‡Full Professor, Physics Department, pegoraro@df.unipi.it.
§Full Professor, Aerospace Engineering Department, CEO Alta S.p.A., m.andrenucci@alta-space.com.

configurations and scales) lower thrust levels but higher thrust efficiency at lower power levels. SF-MPD thrusters, should also offer the possibility of throttling the thrust level (by tuning the imposed current) independently of the specific impulse level (which depends on the ratio between the squared imposed current and the propellant mass flow rate, i.e. $j^2/\dot{m}$). Nonetheless the operation of MPD thrusters has been limited to research laboratories, never entering a space qualification phase. This is both for the huge power required to operate these devices, ranging from hundreds of kW to many MW, and for the strong limitations which have been found to occur during their operation, above which a low thrust efficiency (usually lower than 20%) and the inception of critical unstable regimes at high values of the $J^2/\dot{m}$ ratio. These major issues, both of which are the subjects of extensive literature, indicate the need for further basic research on these devices in order to fully understand the underlying physical mechanisms and to find suitable technological solutions. The interest in the fundamental physics and acceleration mechanisms of MPD thrusters is very important also because of the possibility of employing them, with suitable modifications, as injection stages in fusion devices or plasma accelerators in plasma-surface interaction studies.

The simplest approach to analyse the working principles of these devices is by means of one-dimensional models[1,2,3], in which all the complex physical interactions are reduced to the study of axial variations of the plasma and electromagnetic field quantities. Despite their apparent simplicity, these models have proved effective in providing information on the basics of the acceleration mechanism, as well as in giving an indication of the possible limitations affecting the acceleration process, while maintaining an intriguing combination of simplicity and physical insight.

In this work we aim at performing a semi-analytical analysis of a class of two-dimensional solutions of the steady plasma flow in coaxial SF-MPD thrusters. A set of physical and analytical simplifying assumptions will be introduced in order to reduce the three dimensional problem to an equivalent one-dimensional problem in which the only remaining variable is the current collected at the electrodes.

II. Formulation of the model

In SF-MPD thrusters the main acceleration process is driven by the electromagnetic forces. A simple, yet effective, description of this process can be obtained by considering the magnetohydrodynamic model for steady state plasma flows, which takes into account the mass conservation equation

$$\nabla \cdot (\rho \mathbf{v}) = 0 \tag{1}$$

where ρ represents the plasma density and $\mathbf{v}$ is the flow velocity, and the momentum equation

$$\rho \left(\mathbf{v} \cdot \nabla\right) \mathbf{v} = \frac{1}{c} \mathbf{j} \times \mathbf{B}, \tag{2}$$

where c is the light speed and the electric current, $\mathbf{j}$, is related to the magnetic field, $\mathbf{B}$, by Ampere's law $\mathbf{j} = (c/4\pi) \nabla \times \mathbf{B}$. The plasma is assumed to be fully ionized before the inlet of the acceleration channel and quasi-neutrality is assumed throughout the channel. Moreover, in the momentum equation, Eq. (2), viscous and gas-dynamic effects have been neglected (considerations arising from the inclusion of the gas-dynamic effects in the model are presented in the Sec. IV).

In addition to the two equations (1)-(2), the momentum balance on the electrons can be expressed in terms of the Ohm's equation

$$\mathbf{E} + \frac{1}{c} \mathbf{v} \times \mathbf{B} = \frac{\mathbf{j}}{\sigma} \tag{3}$$

where a finite, yet constant, conductivity σ is introduced in order to describe the (dissipative) collisional phenomena.

Introducing a system of cylindrical coordinates (r, ϕ, z), the geometry of the thruster is characterized by two coaxial cylindrical electrodes, where r_a is the radius of the outer electrode (anode) and r_c is the radius of the inner electrode (cathode).

Among the equilibria described by the set of Eqs. (1)-(3), a special class of solutions is represented by flows which are in the axial direction only. Neglecting the radial velocity, the mass conservation equation can be written as

$$\frac{\partial}{\partial z} \left(\rho v_z\right) = 0 \;\Rightarrow\; \rho v_z = F\left(r\right), \tag{4}$$

where v_z is the axial velocity and the function F represents the mass flow rate at a given radius, which is constant (through the channel) on each flow streamline. The radial component of Eq. (2) yields

$$\frac{\partial}{\partial r}\left(rB_\phi\right) = 0 \;\Rightarrow\; dB_\phi = -\frac{2I}{cr}, \tag{5}$$

where $I = I\left(z\right)$ represents the overall current that flows inside the cathode at a given axial position. Inside the plasma, the current density is thus in the radial direction only,

$$j_r = \frac{c}{4\pi}\frac{\partial B_\phi}{\partial z}, \tag{6}$$

and the axial component of the momentum equation results

$$\frac{\partial}{\partial z}\left(\rho v_z^2 + \frac{1}{8\pi}B_\phi^2\right) = 0 \;\Rightarrow\; \rho v_z^2 = J\left(r\right) - \frac{1}{8\pi}B_\phi^2. \tag{7}$$

By introducing an electric potential $\mathbf{E} = -\nabla V$, from the axial component of Eq. (3) we obtain

$$\frac{\partial V}{\partial z} = 0 \;\Rightarrow\; V = V\left(r\right), \tag{8}$$

and the radial component of the Ohm's equation yields

$$-\frac{\partial V}{\partial r} - \frac{1}{c}v_z B_\phi = -\frac{1}{\sigma}\frac{c}{4\pi}\frac{\partial B_\phi}{\partial z}. \tag{9}$$

By substituting Eqs. (4)-(8) into Eq. (9), we obtain a first-order ordinary differential equation for the cathode current

$$\frac{c}{2\pi r\sigma}\frac{\mathrm{d}I}{\mathrm{d}z} = -\frac{1}{\pi c^3 r^3 F}I^3 + \frac{2J}{crF}I + cV', \tag{10}$$

were the notation $V' = \mathrm{d}V/\mathrm{d}r$ has been introduced. The boundary condition associated with Eq. (10) can be deduced by imposing that the current flows only between the two electrodes with no losses outside the acceleration channel. In these conditions, which are appropriated for steady-state operations, the trailing edge of the anode corresponds to the point where the current vanishes and thus the boundary condition can be expressed as

$$I\left(z_{\mathrm{out}}\right) = 0\,. \tag{11}$$

Since Eq. (10) needs to be satisfied at each radius, the coefficients of each term should be independent from the radial position. This implies a constraint on the choice of the functions F, J and V', which results in the expressions

$$F = \frac{\dot{m}}{2\pi \ln\frac{r_a}{r_c}}\frac{1}{r^2}, \qquad J = \frac{J_0}{2\pi \ln\frac{r_a}{r_c}}\frac{1}{r^2}, \qquad V' = \frac{\Delta V}{\ln\frac{r_a}{r_c}}\frac{1}{r}, \tag{12}$$

where $\dot{m}$ represents the overall mass flow rate

$$\dot{m} = 2\pi\int \rho v_z r\mathrm{d}r = 2\pi\int Fr\mathrm{d}r, \tag{13}$$

J_0 is the outflow of momentum at the outlet

$$J_0 = 2\pi\int Jr\mathrm{d}r = \dot{m}v_z^{out} \tag{14}$$

and ΔV is the electric potential difference between the two electrodes

$$\Delta V = \int V'\mathrm{d}r. \tag{15}$$

By using Eq. (12) and introducing a characteristic current value, according to Maecker's equation[4],

$$I^* = \left(\frac{c^2 J_0}{\ln\frac{r_a}{r_c}}\right)^{1/2}, \tag{16}$$

the dimensionless form of the differential equation (10) becomes

$$\frac{\mathrm{d}y}{\mathrm{d}x} = y^3 - y + b, \qquad y\,(0) = 0, \tag{17}$$

where $y = I/I^*$ represents the scaled current and $x = a(z_{\mathrm{out}} - z)/L$ is a dimensionless axial coordinate which is zero on the outlet surface and increases toward the inlet (L is a typical scale length of the device). The Eq. (17), which is characterized by the two dimensionless parameters

$$a = \frac{4\pi\sigma L J_0}{c^2 \dot{m}}, \qquad b = \frac{c}{2}\frac{\dot{m}\Delta V}{J_0^{3/2}}\left(\ln\frac{r_a}{r_c}\right)^{-1/2}, \tag{18}$$

can be solved by integrating

$$\int_0^y \frac{\mathrm{d}\xi}{\xi^3 - \xi + b} = x. \tag{19}$$

Notice that the parameter a can be rewritten by using Eq. (14) as $a = \left(4\pi/c^2\right)\sigma L v_{out}$, which represents the magnetic Reynolds number of the flow. In order to evaluate the integral on the left side of Eq. (19) a distinction is needed between those values of the voltage parameter b for which the integrand presents a singularity and those for which the integrand is regular. Indeed, if the denominator of the integrand becomes zero at a certain current value, i.e. if and only if the third order polynomial

$$\xi^3 - \xi + b = 0 \tag{20}$$

has a positive real root, a singularity arises. It is easy to show that this condition is only satisfied if the roots of Eq. (20) are all real, which corresponds to the condition

$$b^2 \leq \frac{4}{27}. \tag{21}$$

If the integrand of Eq. (19) has a singularity, the solution is of the type shown in Fig. 1-(a), where the dimensionless current y is plotted versus the scaled distance from the outlet, x.

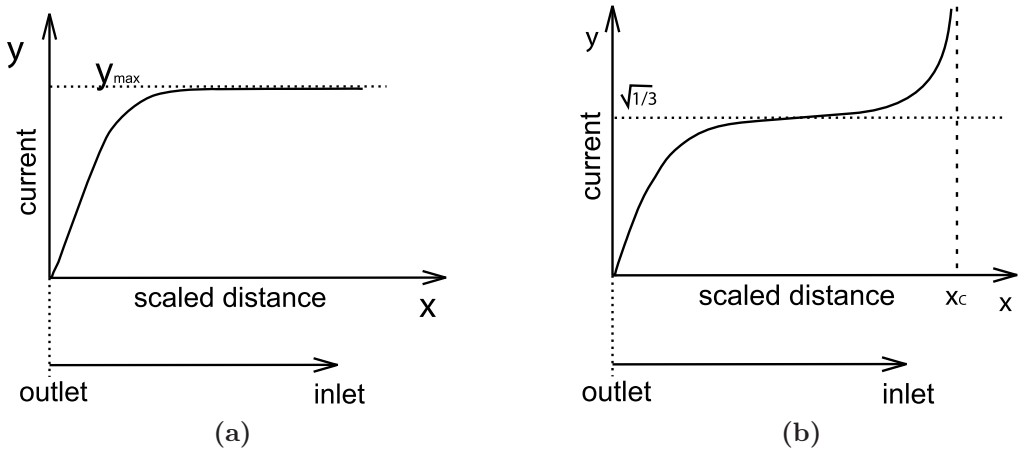

Figure 1: Behaviour of the solution for (a) $b^2 < 4/27$ and (b) $b^2 \geq 4/27$. The dimensionless current, y, is plotted versus the scaled distance from the outlet, x.

By changing the parameter a the solution illustrated in Fig. 1-(a) is simply scaled with respect to the axis x and this shows that the increase of plasma conductivity yields to the concentration of the current density in a small layer at the outlet (see Martinez-Sanchez[2] for further discussion about this point).

The current increases from the exit of the thruster up to an asymptotic value and, in these conditions, the overall current that flows through the thruster, which corresponds to the value of $y\,(x_{\mathrm{out}} = a)$, is bounded by

$$y_{\max} = \frac{2}{\sqrt{3}}\sin\theta, \qquad \text{with} \quad \theta = \frac{\pi}{6} - \frac{1}{3}\arctan\left(\sqrt{\frac{4}{27b^2} - 1}\right). \tag{22}$$

Consequently, since the dimensionless expression of the flow velocity can be written as

$$v_z/v_z^{out} = 1 - y^2, \tag{23}$$

where $v_z^{out} = J_0/\dot{m}$ is the outlet velocity, the scaled thrust results

$$T/J_0 = \dot{m}\left(v_z^{out} - v_z\right)/J_0 \leq y_{\max}^2 \tag{24}$$

where $y_{\max}$ is given in Eq. (22), leading to $T/J_0 < 1/3$.

From the operational point of view, this kind of solutions has a critical behaviour when the thruster is operated at an overall current close to the asymptotic value. As the total current fixes the inlet (dimensionless) position, in this case this position will undergo great variations as a consequence of tiny perturbations of the parameters, leading to possible unstable/unsteady behaviour.

For $b^2 > 4/27$ the only real root of Eq. (20) is negative and thus in the integration domain the integrand in Eq. (19) is always positive and non-singular. In Fig. 1-(b) a typical solution is illustrated in terms of the dimensionless current and of the scaled distance. In these solutions a vertical asymptote exists at a point x_c and here the solution diverges as

$$y \propto \sqrt{\frac{1}{x - x_c}}. \tag{25}$$

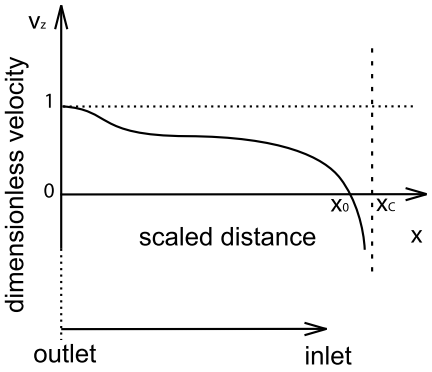

Figure 2: Behaviour of the dimensionless velocity for $b^2 > 4/27$. The velocity v_z/v_z^{out} is plotted versus the scaled distance from the outlet, x.

The plasma velocity, which is defined by Eq. (23), is illustrated in Fig. 2, where the dimensionless velocity is plotted versus the scaled distance from the outlet. This figure shows that the velocity decreases from the outlet inward, as expected, and that also for the velocity a vertical asymptote exists at $x = x_c$. However, at a critical length $x_0 < x_c$ from the outlet the velocity becomes zero and for $x \geq x_0$ the solution has no physical meaning anymore. By varying the voltage parameter b the position of the critical length varies as shown in Fig. 3.

A. Calculation of losses and efficiency

The power losses due to the resistive phenomena in the plasma can be analysed by considering that, from the momentum equation it results

$$\frac{\partial}{\partial z}\frac{v_z^2}{2} + \frac{1}{4\pi}\frac{B_\phi}{\rho}\frac{\partial B_\phi}{\partial z} = 0, \tag{26}$$

and by substituting Ohm's equation (9) in the form

$$\frac{B_\phi}{\rho} = -\frac{cV'}{F} + \frac{1}{\sigma F}\frac{c}{4\pi}\frac{\partial B_\phi}{\partial z}, \tag{27}$$

it follows that

$$\frac{\partial}{\partial z}\left(\frac{v_z^2}{2} - \frac{1}{4\pi}\frac{cV'}{F}B_\phi\right) = -\frac{1}{\sigma cF}\left(\frac{c}{4\pi}\frac{\partial B_\phi}{\partial z}\right)^2 = -\frac{j^2}{\sigma F}. \tag{28}$$

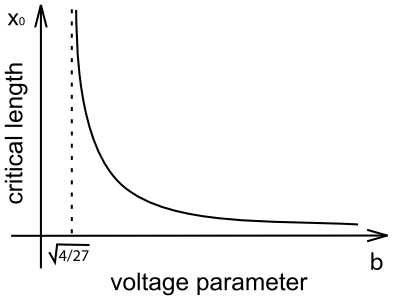

Figure 3: The critical length x_c (in dimensionless form) is plotted as a function of the voltage parameter b.

By using Eq. (23) for the velocity and considering the dimensionless representation introduced before, the power losses can be written as

$$P_{loss} = \int \frac{j^2}{\sigma}\mathrm{d}V = \frac{J_0^2}{2\dot{m}}\left(y_{\rm in}^4 - 2y_{\rm in}^2 + 4by_{\rm in}\right), \tag{29}$$

where $y_{\rm in}$ represents the overall current that flows throughout the channel region (for $z = z_{\rm in}$, $x = a(z_{\rm out} - z_{\rm in})/L$). The efficiency of the thruster, which is defined as the ratio between the input electric power and the variation of the flow kinetic energy, results

$$\eta = 1 - \frac{P_{loss}}{I_{tot}\Delta V}, \tag{30}$$

and by substituting Eq. (29) we obtain

$$\eta = \frac{2y_{\text{in}} - y_{\text{in}}^3}{4b}. \tag{31}$$

In the definition given above the efficiency shows a dependence on the voltage parameter and on the overall current, which is directly related to the distance from the outlet, i.e. on the scaled channel length in the dimensionless system.

Provided that $a < x_c$ (i.e. the channel length, resulting by the total imposed current, is smaller than the critical length x_c) and given a voltage parameter b, the efficiency has a maximum for an imposed current equal to $y_{\text{in}} = \sqrt{2/3}$ and for this value the efficiency results

$$\eta = \frac{\sqrt{2/27}}{b}. \tag{32}$$

For $b^2 \leq 4/27$ the maximum value of y_{in} is related to the voltage parameter by Eq. (22) and it can be shown that for these operating conditions it is always $y_{\text{in}} < \sqrt{1/3}$ and $\eta < 5/8$. For $b^2 > 4/27$ the maximum of Eq. (32), which is reached for $b^2 \to 4/27$ and $x \to \infty$, has the value

$$\eta_{\max} = \frac{\sqrt{2}}{2}. \tag{33}$$

In Fig. 4 is represented the efficiency as a function of the scaled channel length and of the voltage parameter. For $b^2 > 4/27$, the domain in which the efficiency is plotted correspond to points below the critical length illustrated in Fig. 3.

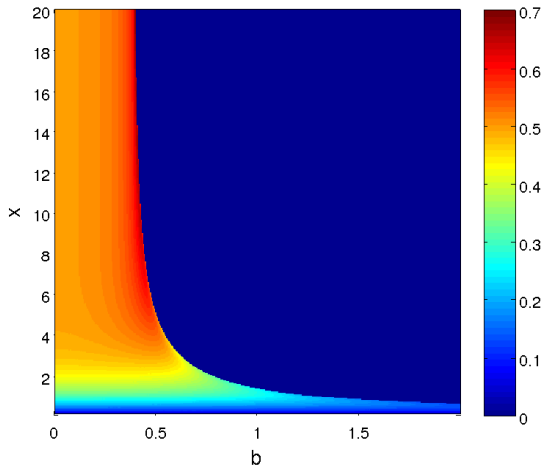

Figure 4: Parametric dependence of thrust efficiency in the cold MHD case.

The maximum efficiency found in this "cold" MHD cylindrical case, $\eta_{\max} = \sqrt{2}/2$, is slightly higher ($\sim 6\%$) than the corresponding value obtained by Kuriki et al.[1] (as well as in other works on an analogous case[2,3]), i.e. $\eta_{\max} = 3\sqrt{3}/8$. This difference comes from the fact that we take into account how a particular solution, i.e. a particular choice of the free parameters, changes the value of the inlet velocity, while Kuriki et al. always assumed a zero inlet velocity, as already noticed by Martinez-Sanchez[2].

III. Special case: MHD flow in conical geometry

As an extension to the previous analysis of the "cold" MHD flow in a cylindrical geometry, we deal now with the case of a conical channel, i.e. a channel with conical anode and cathode. We retain the previously described simplifying assumptions on the flow. Calculations are performed in a spherical coordinate system (r, θ, ϕ) in which the inlet section is denoted by the radial coordinate r_{in} while the outlet section is denoted by r_{out}. The position of the electrodes is determined by the following values of the polar coordinate θ: θ_c

stands for the cathode while θ_a stands for the anode. The flow velocity is everywhere aligned along $\hat{r}$, while the current density vector has its only non-zero component along $\hat{\theta}$.

The continuity equation reads

$$\frac{1}{r^2}\frac{\partial(r^2\rho u)}{\partial r} = 0 \;\Rightarrow\; \rho u = \frac{F(\theta)}{r^2} \tag{34}$$

while from the radial momentum equation it follows:

$$\frac{1}{r^2}\frac{\partial(r^2\rho u^2)}{\partial r} = -\frac{B_\phi}{4\pi r}\left[\frac{\partial(rB_\phi)}{\partial r}\right] \;;$$

which can be recast as

$$\frac{\partial}{\partial r}\left[r^2\left(\rho u^2 + \frac{B_\phi^2}{8\pi}\right)\right] = 0 \;\Rightarrow\; \rho u^2 + \frac{B_\phi^2}{8\pi} = \frac{J(\theta)}{r^2} \tag{35}$$

and then

$$u = \frac{J(\theta)}{F} - \frac{r^2 B_\phi^2}{8\pi F} \;. \tag{36}$$

The momentum equation along $\hat{\theta}$ gives

$$\frac{1}{r}\frac{\partial(B_\phi^2/2)}{\partial\theta} + \frac{\cot\theta B_\phi^2}{r} = 0$$

which can be integrated by separation of variables imposing proper boundary conditions

$$B_\phi = -\frac{2I(r)}{cr\sin\theta} \;. \tag{37}$$

Taking the radial component of Ohm's equation we obtain

$$\frac{\partial V}{\partial r} = 0 \;\Rightarrow\; V = V(\theta) \tag{38}$$

while the azimuthal component leads to

$$-\frac{1}{r}\frac{\partial V}{\partial\theta} - \frac{uB_\phi}{c} = -\frac{c}{4\pi\sigma r}\frac{\partial(rB_\phi)}{\partial r} \;. \tag{39}$$

By substitution of the previous expressions into Eq. (39) we find

$$\frac{1}{\sigma}\frac{\mathrm{d}I}{\mathrm{d}r} = \frac{4\pi J}{c^2 F}I - \frac{2}{c^4 F\sin^2\theta}I^3 - 2\pi\sin\theta V' \,, \qquad I(r_{\mathrm{out}}) = 0 \;. \tag{40}$$

In order to eliminate the dependence of F, J and V' on θ we choose

$$F = \frac{\dot{m}}{2\pi\ln\left[\dfrac{\tan(\theta_a/2)}{\tan(\theta_c/2)}\right]}\frac{1}{\sin^2\theta} \,, \quad J = \frac{J_0}{2\pi\ln\left[\dfrac{\tan(\theta_a/2)}{\tan(\theta_c/2)}\right]}\frac{1}{\sin^2\theta} \,, \quad V' = \frac{\mathrm{d}V}{\mathrm{d}\theta} = \frac{\Delta V}{\ln\left[\frac{\tan(\theta_a/2)}{\tan(\theta_c/2)}\right]}\frac{1}{\sin\theta}$$

as

$$\begin{aligned}
\dot{m} &= 2\pi\int \rho u r^2\sin\theta\,\mathrm{d}\theta = 2\pi\int F\sin\theta\,\mathrm{d}\theta \\
J_0 &= 2\pi\int\left(\rho u^2 + \frac{B_\phi^2}{2\mu_0}\right)r^2\sin\theta\,\mathrm{d}\theta = 2\pi\int Jr^2\sin\theta\,\mathrm{d}\theta \\
\Delta V &= \int\frac{1}{r}\frac{\mathrm{d}V}{\mathrm{d}\theta}r\,\mathrm{d}\theta
\end{aligned}$$

where we made use of the previously defined quantities.

It can be verified (assuming a constant current density distribution along the channel) that the equivalent Maecker's formula for the thrust of a SF-MPD thruster in conical geometry is

$$J_0 = \frac{(I^*)^2}{c^2} \ln\left[\frac{\tan(\theta_a/2)}{\tan(\theta_c/2)}\right]$$

from which it follows

$$I^* = \sqrt{\frac{c^2 J_0}{\ln\left[\frac{\tan(\theta_a/2)}{\tan(\theta_c/2)}\right]}}$$

Next we substitute the expressions for quantities F, J and V', and then normalize Eq. (40) introducing the dimensionless quantities $y = I/I^*$ and $x = a(r_{\text{out}} - r)/L$

$$\frac{\mathrm{d}y}{\mathrm{d}x} = y^3 - y + b \tag{41}$$

where the following parameters have been introduced

$$a = \frac{4\pi\sigma L J_0}{c^2 \dot{m}}, \quad b = \frac{c}{2}\frac{\dot{m}\Delta V}{J_0^{3/2}} \ln^{-1/2}\left[\frac{\tan(\theta_a/2)}{\tan(\theta_c/2)}\right]$$

which are equal (a) or analogous (b) to those introduced in the previous section.

These calculations have shown that if gasdynamic contributions are neglected, the problem in conical geometry is completely equivalent to the problem in cylindrical geometry.

IV. Cylindrical geometry with gasdynamic contributions

In this section we investigate the gasdynamic contributions to the flow, i.e. we retain all the assumptions previously made but for a finite plasma temperature, which requires the addition of an energy conservation equation. We treat the plasma as an ideal gas. Following the analysis made in Sec. II, we obtain the for the continuity equation

$$\frac{\partial}{\partial z}(\rho v_z) = 0 \;\Rightarrow\; \rho v_z = F(r)\,; \tag{42}$$

for radial momentum equation

$$\frac{\partial}{\partial r}(r B_\phi) = 0 \;\Rightarrow\; B_\phi = -\frac{2I(z)}{cr}; \tag{43}$$

and for the axial momentum equation

$$\frac{\partial}{\partial z}\left(\rho v_z^2 + \frac{1}{8\pi}B_\phi^2 + p\right) = 0 \;\Rightarrow\; \rho v_z^2 = J(r) - \frac{1}{8\pi}B_\phi^2 - p\,. \tag{44}$$

The axial component of the Ohm equation results

$$\frac{\partial V}{\partial z} = 0 \;\Rightarrow\; V = V(r)\,; \tag{45}$$

while the radial component is

$$-\frac{\partial V}{\partial r} - \frac{1}{c}v_z B_\phi = -\frac{1}{\sigma}\frac{c}{4\pi}\frac{\partial B_\phi}{\partial z}. \tag{46}$$

In addition, the conservation of total enthalpy is expressed by

$$\frac{\partial}{\partial z}\left(\frac{v_z^2}{2} + h - \frac{1}{4\pi}\frac{cV'}{F}B_\phi\right) = 0 \;\Rightarrow\; h = \frac{\gamma}{\gamma-1}\frac{p}{\rho} = H(r) - \frac{v_z^2}{2} + \frac{1}{4\pi}\frac{cV'}{F}B_\phi; \tag{47}$$

where $h = \frac{\gamma}{\gamma-1}\frac{p}{\rho}$ is the internal enthalpy for an ideal gas.

Combining Eqs. (44)-(47) we get an algebraic equation for the axial velocity

$$\frac{\gamma+1}{2\gamma}v_z^2 - \left(\frac{J}{F} - \frac{1}{8\pi F}B_\phi^2\right)v_z + \frac{\gamma-1}{\gamma}\left(H + \frac{1}{4\pi}\frac{cV'}{F}B_\phi\right) = 0\,. \tag{48}$$

By substituting Eqs. (42)-(45) into Eq. (46) and taking into account that from Eq. (48)

$$v_z = \left(\frac{2\gamma}{\gamma+1}\right)\left[\frac{J}{2F} - \frac{1}{16\pi F}B_\phi^2 \pm \sqrt{\left(\frac{J}{2F} - \frac{1}{16\pi F}B_\phi^2\right)^2 - \frac{\gamma^2-1}{2\gamma^2}\left(H + \frac{1}{4\pi}\frac{cV'}{F}B_\phi\right)}\right], \tag{49}$$

we get

$$\frac{1}{\sigma}\frac{c^2}{4\pi}\frac{\partial B_\phi}{\partial z} = -\gamma^*\frac{1}{16\pi F}B_\phi^3 + \gamma^*\frac{J}{2F}B_\phi + cV' \pm \gamma^* B_\phi\sqrt{\left(\frac{J}{2F} - \frac{1}{16\pi F}B_\phi^2\right)^2 - \frac{\gamma^2-1}{2\gamma^2}\left(H + \frac{1}{4\pi}\frac{cV'}{F}B_\phi\right)}, \qquad B_\phi(r,L) = 0\,, \tag{50}$$

where $\gamma^* = 2\gamma/(\gamma+1)$, the boundary condition coming from the assumption that no current line extends beyond the thruster exit section. From Eq. (50), making use of Eq. (43), a first order ordinary differential equation is obtained which describes the variation of the current $I(z)$ collected at the cathode along z:

$$\frac{c}{2\pi r\sigma}\frac{\mathrm{d}I}{\mathrm{d}z} = -\frac{\gamma^*}{2\pi c^3 r^3 F}I^3 + \frac{\gamma^* J}{crF}I - cV' \pm \frac{2\gamma^* I}{cr}\sqrt{\left(\frac{J}{2F} - \frac{1}{4\pi c^2 r^2 F}I^2\right)^2 - \frac{\gamma^2-1}{2\gamma^2}\left(H - \frac{1}{2\pi r}\frac{V'}{F}I\right)}, \qquad I(L) = 0\,. \tag{51}$$

In order for the coefficients of Eq. (51) not to depend on r, we choose

$$F = \frac{\dot m}{2\pi \ln\frac{r_a}{r_c}}\frac{1}{r^2}, \qquad J = \frac{J_0}{2\pi\ln\frac{r_a}{r_c}}\frac{1}{r^2}, \qquad H = \frac{\gamma\gamma^*}{\gamma-1}h_0^2 \qquad V' = \frac{1}{r}\frac{\Delta V}{\ln\frac{r_a}{r_c}}, \tag{52}$$

where the following definitions for the propellant mass flow rate

$$\dot m = 2\pi\int \rho v_z r\mathrm{d}r = 2\pi\int Fr\mathrm{d}r\,, \tag{53}$$

the potential difference between the electrodes

$$\Delta V = \int V'\mathrm{d}r\,, \tag{54}$$

and the sound velocity

$$c_s^2 = \frac{\gamma p}{\rho} \tag{55}$$

have been used. The quantity

$$I^* = \left(\frac{c^2 J_0}{\ln\frac{r_a}{r_c}}\right)^{1/2}, \tag{56}$$

is used to normalize the current collected at the cathode and then Eq. (51) can be rewritten as

$$\frac{\mathrm{d}y}{\mathrm{d}x} = \frac{1}{2}\left(y^3 - y + 2b \mp y\sqrt{(y^2-1)^2 - d^2 + 8\left(\frac{\gamma-1}{\gamma}\right)by}\right), \qquad y(0) = 0\,, \tag{57}$$

where $y = I/I^*$ is the dimensionless current, $x = a(z_{\mathrm{out}} - z)/L$ and the following expressions hold

$$a = \frac{4\pi\sigma L\gamma^* J_0}{c^2\dot m}, \qquad b = \frac{c}{2}\frac{\dot m\Delta V}{\gamma^* J_0^{3/2}}\left(\ln\frac{r_a}{r_c}\right)^{-1/2}, \qquad d = \frac{2\dot m h_0}{J_0} \tag{58}$$

Eq. (57) can be solved by separation of variables:

$$\int_0^y \frac{2\mathrm{d}\xi}{\xi^3 - \xi + 2b \mp \xi\sqrt{(\xi^2-1)^2 - d^2 + 8b\xi(\gamma-1)/\gamma}} = a\frac{x}{\varepsilon}\,. \tag{59}$$

As

$$\left(\xi^2-1\right)^2 - d^2 + 8b\xi\left(\gamma-1\right)/\gamma \geq 0 \tag{60}$$

$$0 \leq d \leq 1, \tag{61}$$

(the limits on d are obtained by evaluating the previous expression in $\xi = 0$ and $\xi = 1$) the denominator of the expression inside the integral is zero for

$$\left(\frac{2-\gamma}{\gamma}\right)\xi^3 + \frac{d^2}{4b}\xi^2 - \xi + b = 0 \tag{62}$$

which has three solutions if

$$0 < b^2 \leq \frac{-\left(9d^2-8\right)+\left(4-3d^2\right)^{3/2}}{108}\left(\frac{\gamma}{2-\gamma}\right) \qquad \text{and} \qquad 0 \leq d^2 < 1\,, \tag{63}$$

giving indication that, as gasdynamic effects become more important, i.e. $d \to 1$, the interval of the parameter b for which the integral in Eq. (59) has a singularity tends to zero.

A. Solutions with horizontal asymptote

If the integrand in Eq. (59) has a singularity, the solution for the dimensionless current will present a horizontal asymptote for increasing values of x. Following the analysis made in the case with no gasdynamic effects, we skip in this case a detailed analysis of these solutions because they are not effective from the propulsive standpoint, as they correspond to very small acceleration of the flow. In this section we want to identify in what cases we can find this kind of solutions.

Recall that Eq. (62) is obtained by setting to zero the denominator of Eq. (59), which has two blocks: the cubic expression $\xi^3-\xi+2b$ and the square root term. The cubic term must be coherent with the choice made of the sign in front of the square root when we set to zero the entire expression, for all the y values from 0 to the value corresponding to total current (in case of a solution without the horizontal asymptote) or the first value in correspondence of which the denominator of Eq. (59) goes to zero (in case of a solution with a horizontal asymptote), which we will call $\tilde{y} \equiv \tilde{\xi}$. This just means that, for example, if we choose the positive sign in front of the square root term and set to zero the entire denominator of the integrand, then the cubic term $\xi^3 - \xi + 2b$ must accordingly be negative.

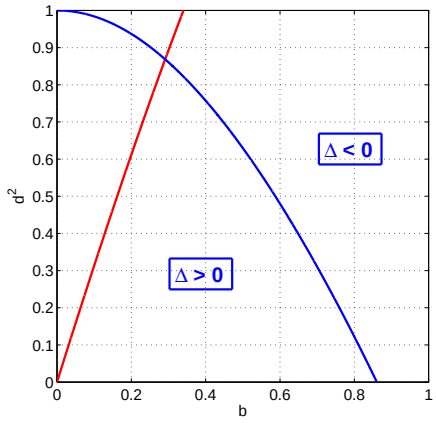

Figure 5: Parameter choices for: smooth sonic transition (red) and the discriminant of Eq. (62) to be zero (blue).

1. *Positive square root term*

In this case it must be verified that

$$\xi^3 - \xi + 2b < 0 \qquad \forall\, \xi \in \left[0, \tilde{\xi}\right] \tag{64}$$

$\tilde{\xi}$ being the first positive root of Eq. (62). The cubic $\xi^3-\xi+2b$ can have one negative real root or three real roots, two of which are positive (Descartes' rule of signs). In the first case the cubic is always positive for positive values of ξ, i.e. of y. In the second case, in order to fulfil Eq. (64), the first non-negative root should actually be equal to zero and the second non-negative root should be greater than y_{in}; as it is impossible to have a root equal to zero for $b > 0$, it follows that it is impossible, in any case, to fulfil Eq. (64), so if we choose the positive sign in front of the square root term we always find solutions without a horizontal asymptote.

2. *Negative square root term*

According to what we have previously said, the presence of a root of Eq. (62) is coherent with

$$\xi^3 - \xi + 2b \geq 0 \qquad \forall\, \xi \in \left[0, \tilde{\xi}\right]$$

in case the cubic $\xi^3 - \xi + 2b$ has only one negative real solution or in case there are three real roots whose smallest positive one is greater than $\tilde{\xi}$. It can be verified that this is always the case. This means that if we choose the positive sign in front of the square root term, and if Eq. (62) has a positive root, we will find solutions with a horizontal asymptote.

B. Conditions for smooth sonic transitions

The sign in front of the square root in Eq. (59) identifies the subsonic/supersonic branches of the solution. Then, the sonic transition occurs when the expression inside the square root becomes zero, as in that case the two branches coincide. As the cited expression must be a non-negative quantity, it can only become zero in correspondence of a maximum or minimum as a function of ξ. The condition for the ξ-derivative of the terms inside the square root to be zero is

$$b = \frac{\gamma}{2(\gamma-1)}\xi(1-\xi^2) \, .$$

Substitution of this expression in the radicand leads to

$$d^2 = -3\xi^4 + 2\xi^2 + 1 = -(\xi^2 - 1)(3\xi^2 + 1) \, .$$

If we set the value of the dimensionless current at the sonic (transition) point, i.e. $\xi_* \equiv y_*$, the two previous expressions give the values of b and d^2 in order for the transition to be possible and smooth, i.e. without any discontinuity in the solution. By varying the value of ξ at the transition point, we can trace a curve on the plane $b - d^2$ which represents the possible pairs allowing for a smooth transition through the sonic point. In Fig. 5 this curve is shown in red, superposed to the curve (blue) giving the values for which the discriminant of Eq. (62). In order to always find regular solutions (with no asymptote in the current) for both choices of the sign in front of the square root term in Eq. (59), the entire denominator in that equation must not vanish for positive values of ξ (i.e. of the current y) and then its discriminant must be negative. This implies that the only $b - d^2$ pairs leading to regular solutions with a smooth sonic transition are those corresponding to the piece of red curve lying above the blue one. This is equivalent to saying that the sonic transition can only happen in correspondence of a normalized current value in the range $[\sqrt{2/3}, 0.8525]$.

The higher the b-value the higher the d-value, i.e. higher values of b correspond to operating regimes in which gasdynamic contributions have a greater relative importance with respect to electromagnetic ones.

C. Solutions

By performing the integration of Eq. (59) it is possible to obtain the dependence of the dimensionless current y along the dimensionless length of the channel. The profiles of the normalized collected current, current density, and of the two (subsonic/supersonic) branches of the velocity are shown in Fig. 7, corresponding to the two extreme possible regimes, i.e. with $b = b_{\min}$ and $b = b_{\max}$.

It is important to find the values of the dimensionless current where the (subsonic) flow velocity becomes zero. From Eq. (49) we obtain the subsonic branch of the solution:

$$v_{\rm sub} = \frac{\gamma}{\gamma+1}\frac{J_0}{\dot{m}} \underbrace{\left[(1-y^2) - \sqrt{(1-y^2)^2 - d^2 + 8b\frac{\gamma-1}{\gamma}y}\right]}_{=\overline{v}_z}$$

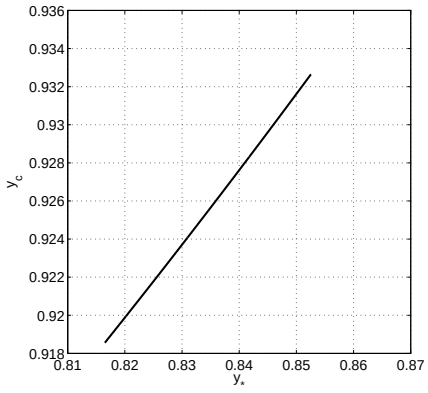

Figure 6: Maximum allowed values of dimensionless total current in order to have regular solutions with smooth sonic transition.

Set this expression to zero, and substituting the values of b and d^2 as a function of y at the sonic point, y_*, we find $y_c = (3y_* + 1)/(4y_*)$. This trend is shown in Fig. 6. Once we choose a particular solution by choosing the value y_* (or b or d^2), we can only find regular solutions with a smooth sonic transition if the (dimensionless) current which is imposed to the thruster is lower than the y_0 value corresponding to the chosen y_*.

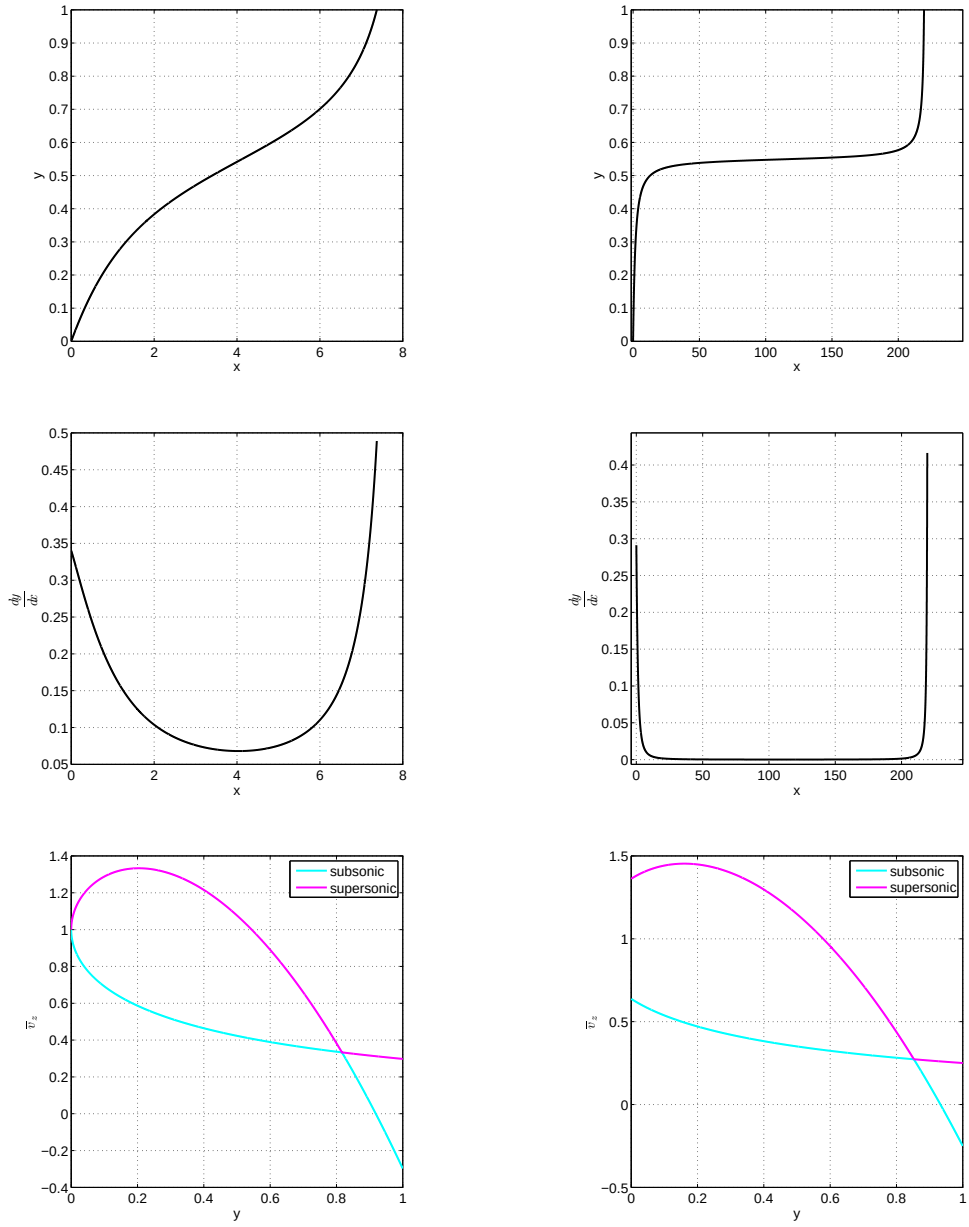

Figure 7: Profiles of collected current (y), current density $\left(\left(\frac{\partial y}{\partial X}\right)^{-1}\right)$, and of the two (subsonic/supersonic) branches of the velocity $\left(\left[(1-y^2) \mp \sqrt{(1-y^2)^2 - d^2 + 8b\frac{\gamma-1}{\gamma}y}\right]\right)$ corresponding to $b = b_{\min}$ (right) and $b = b_{\max}$ (left).

In Fig. 8 the relative distance between the sonic section and the section in which the flow velocity becomes zero is plotted. This is a very small distance, i.e. the flow becomes sonic in the vicinity of the inlet section, in accordance with analogous results previously obtained[2].

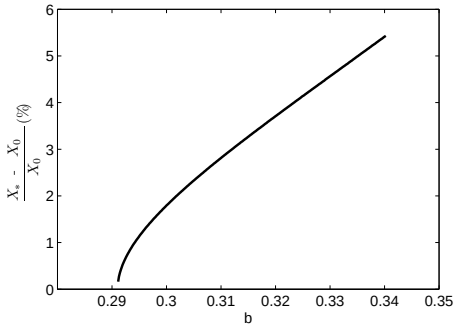

Figure 8: Maximum relative distance (%) of sonic section from inlet.

D. Calculation of losses and efficiency

The volumetric ohmic power loss is

$$\frac{j^2}{\sigma} = \frac{1}{\sigma}\frac{c^2}{16\pi^2}\frac{4}{c^2 r^2}\frac{c^2 J_0}{\ln(r_a/r_c)}\left(\frac{\partial y}{\partial z}\right)^2$$

so the power loss because of the Joule effect is

$$P_{loss} = \frac{c^2 J_0}{2\pi\sigma}\int_0^L \left(\frac{\mathrm{d}y}{\mathrm{d}z}\right)^2 \mathrm{d}z = \frac{c^2 J_0}{2\pi\sigma L}\frac{a}{\epsilon}\int_0^{x_{\rm in}} \left(\frac{\mathrm{d}y}{\mathrm{d}x}\right)^2 \mathrm{d}x\ .$$

The total electrical power feeding the thruster is equal to the volume integral of

$$jE = \frac{c}{4\pi}\frac{2}{cr}\frac{cJ_0^{1/2}}{(\ln(r_a/r_c))^{1/2}}\frac{\mathrm{d}y}{\mathrm{d}z}\frac{\Delta V}{\ln(r_a/r_c)r}$$

which is

$$\begin{aligned} P_{tot} &= \int_0^L \frac{c\Delta V J_0^{1/2}}{(\ln(r_a/r_c))^{1/2}}\frac{\mathrm{d}y}{\mathrm{d}z}\,\mathrm{d}z \\ &= -\frac{c\Delta V J_0^{1/2}}{(\ln(r_a/r_c))^{1/2}}\int_0^{x_{\rm in}} \frac{\mathrm{d}y}{\mathrm{d}x}\,\mathrm{d}X \\ &= -\frac{c\Delta V J_0^{1/2}}{(\ln(r_a/r_c))^{1/2}} y(x_{\rm in}) \end{aligned}$$

from which it follows

$$\eta = 1 - \frac{1}{b}\frac{\displaystyle\int_0^{x_{\rm in}} \left(\frac{\mathrm{d}y}{\mathrm{d}x}\right)^2 \mathrm{d}x}{y(x_{\rm in})}\ .$$

In this case with gasdynamic contributions, the maximum efficiency is obtained in correspondence of $b = b_{\min} = \sqrt{2/3}$ and of the maximum attainable thruster length. The numerically evaluated maximum efficiency is in this case $\eta_{\max} \simeq 0.7$. The white line in the figure gives indication of the x value (as a function of b) where the flow velocity becomes zero: only the pairs above this line correspond to solutions with a subsonic/supersonic transition.

V. Limits of the model and the necessity for the axial current

In this Section we analyse a limitation of the model we have described, which demands a deeper insight into the operation of a coaxial cylindrical SF-MPD thruster.

The simplified quasi-1D models available in the literature, e.g. the works of Martinez-Sanchez[1] or Kuriki et al.[2], dealt with parallel-plate configurations. In these types of thrusters the mathematical description of the flow is obtained by writing the governing equations in cartesian coordinates. In those cases, the problem is mathematically equivalent to solving the governing differential equations along a *medium height* of the channel, assuming that none of the flow or electromagnetic variables depends on the transverse coordinates of the channel, i.e. they depend only on the axial coordinate. This implies that it is possible (at least theoretically, and neglecting second order effects) to obtain a quasi-1D flow in a parallel-plate thruster, with the current density orthogonal to the thruster axis.

In the approach herein described, we have tried to solve the two-dimensional differential equations governing the flow. It is evident that, because of the assumptions we have made, there is actually only one

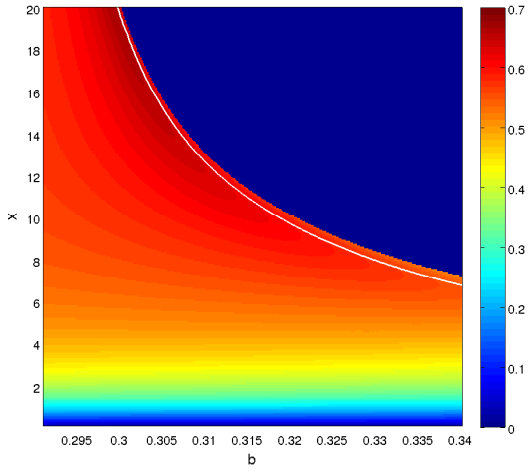

Figure 9: Parametric dependence of thrust efficiency in the case with gasdynamic contributions. The white line in the figure gives indication of the x value (as a function of b) where the flow becomes sonic.

variable, the plasma density, which depends on both the axial and the radial coordinates. This leads to an incoherence of our model, as the radial variation of the magnetic field has been obtained by assuming that all and each of the terms in the radial momentum equation are zero, while the radial dependence of the plasma density implies the presence of an inward-pointing radial gradient of the plasma pressure.

The radial pressure gradient must be compensated for by the presence of an axial component of the current density vector creating a radial component of the Lorentz force. We can estimate how *far* the equilibria we have found are from the actual equilibria by calculating the magnitude of the axial current density which is required to compensate for the radial pressure gradient.

From Eq. (47), making use of previous expressions, we get

$$\begin{aligned} p &= \frac{\gamma-1}{\gamma} h\rho = \frac{\gamma-1}{\gamma} h \frac{F}{v_z} \\ &= \frac{J_0}{4\pi \ln(r_a/r_c)} \left[\frac{d^2}{\hat{v}_z} - \frac{\gamma-1}{\gamma+1}\hat{v}_z - 8\frac{\gamma-1}{\gamma} b \frac{y}{\hat{v}_z} \right] \frac{1}{r^2} \end{aligned}$$

where we introduced $\hat{v}_z = \dfrac{\gamma+1}{\gamma}\dfrac{\dot{m}}{J_0} v_z$. The radial pressure gradient is then equal to

$$\frac{\partial p}{\partial r} = -\frac{J_0}{4\pi \ln(r_a/r_c)} \left[\frac{d^2}{\hat{v}_z} - \frac{\gamma-1}{\gamma+1}\hat{v}_z - 8\frac{\gamma-1}{\gamma} b \frac{y}{\hat{v}_z} \right] \frac{1}{r^3}$$

and from the radial momentum equation we get

$$\begin{aligned} j_z &= -\frac{1}{B_\phi}\frac{\partial p}{\partial r} \\ &= -\frac{c J_0^{1/2}}{8\pi \left(\ln(r_a/r_c)\right)^{1/2}} \left[\frac{d^2}{\hat{v}_z} - \frac{\gamma-1}{\gamma+1}\hat{v}_z - 8\frac{\gamma-1}{\gamma} b \frac{y}{\hat{v}_z} \right] \frac{1}{y}\frac{1}{r^2} \, . \end{aligned}$$

From Ampère's law the following expression for the radial current density can be drawn:

$$j_r = -\frac{c J_0^{1/2}}{2\pi \left(\ln(r_a/r_c)\right)^{1/2}} \frac{1}{Lr} \left(\frac{\partial y}{\partial X} \right) \, .$$

In order to make a comparison, we can rewrite j_z in the as follows:

$$j_z = -\frac{cJ_0^{1/2}}{2\pi\left(\ln(r_a/r_c)\right)^{1/2}}\frac{1}{r^2}\underbrace{\frac{1}{4}\left[\frac{d^2}{\hat{v}_z}-\frac{\gamma-1}{\gamma+1}\hat{v}_z-8\frac{\gamma-1}{\gamma}b\frac{y}{\hat{v}_z}\right]\frac{1}{y}}_{=\hat{j}_z}\ .$$

Fig. 10 shows the profiles of $\hat{j}_z$ in the two extreme possible regimes. Even if the estimated axial current density decreases more rapidly along the radius, it is clear (by comparison with the corresponding $j_r \propto \frac{\mathrm{d}y}{\mathrm{d}x}$ profiles in Fig. 7) that for the greater part of the channel j_z is comparable to j_r (black portion of the curves). It is even greater than j_r near the exit section, where locally the magnetic field goes to zero while the radial pressure gradient to be compensated remains finite, or in the center of the channel in the strong electromagnetic case ($b = b_{\min}$), where the radial current transport is strongly diminished because of the back-electromotive force, even though these considerations do not take into account a possible local radial velocity of the flow.

It is then clear that our results should be taken as *approximate* equilibria, in the sense that they exactly solve the continuity, axial momentum, enthalpy[a] and Ampère's equations, but they do not fulfil exactly the radial momentum balance.

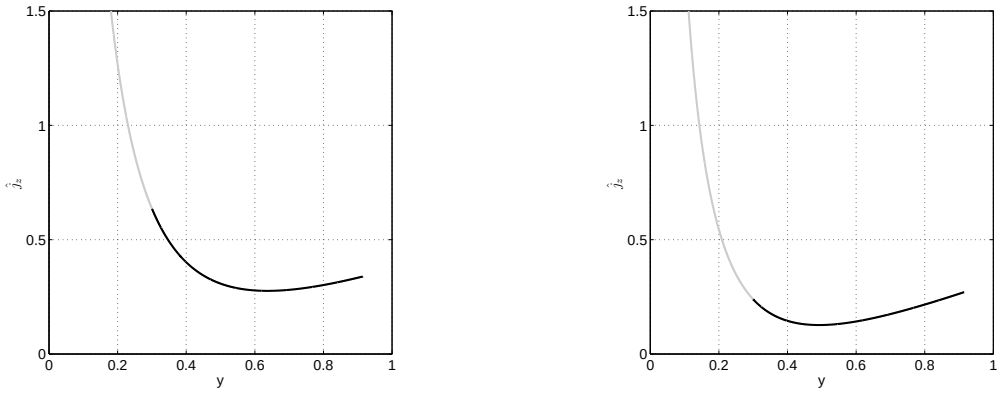

Figure 10: Profile of the dimensionless axial current density $\hat{j}_z$ in the two extreme possible regimes.

On the other hand, these observations give us a deeper insight into the dynamics of the flow in cylindrical SF-MPD thrusters. Our findings implies that there are *topological* reasons, i.e. lying in the very nature of the thruster configuration, which leads to the generation of an axial component of the current density vector, in addition to the presence of a finite electron Hall parameter which is responsible for current lines bending. This suggests that coaxial thruster are even more subject (with respect to parallel-plate thrusters) to the detrimental effects connected to the presence of a pinching component of the Lorentz force, which is widely accepted as one the main causes behind the inception of the onset regime in these thrusters, thus requiring much finer design skills in order to cope with these issues.

VI. Conclusions

The basic plasma acceleration process exploited in self-field MPD thrusters can be described by means of an axisymmetric, resistive, magnetohydrodynamic approach where, as a first approximation, the gasdynamic effects are neglected. Indeed, in the "cold" plasma model described in Sec. II a special class of 2D poloidal equilibria can be introduced for which the problem reduces to an ordinary differential equation. Solutions of this equation allow for a simple analytical description of the flow in terms of two characteristic parameters, the magnetic Reynolds number and a dimensionless parameter which is directly related to the applied voltage. The obtained formulation generalizes the quasi-one-dimensional approach adopted by Kuriki et al.[1] and Martinez-Sanchez[2], whose results can be easily recovered by considering the limit to a planar configuration of the electrodes.

[a] As long as we neglect the electric field line fringing, only the radial current density leads to Ohmic heating.

Modifications induced by gasdynamic pressure on the solutions have been also analysed and a dimensionless parameter that characterizes the gasdynamic effects has been introduced. The requirement of a smooth transition of the flow from subsonic to supersonic regimes yields a relationship between the three characteristic parameters (solutions that satisfy this requirement can thus be characterized in terms of the same two parameters adopted in the "cold" plasma model) and, at the same time, constraints the ranges of parameters for which a smooth transition is possible. Moreover, the smooth sonic transition sets the position of the sonic section close to the inlet section of the acceleration channel.

For both descriptions of the plasma flow, the thrust efficiency has been calculated in terms of the voltage parameter and of the scaled length of the channel. The results of these investigations show that a maximum thrust efficiency exists, whose value is $\eta_{\max} \sim 0.7$ in both cases.

Due to the cylindrical geometry of the channel, the gasdynamic effects, when included in the model, yield an unbalanced force in the radial direction, which can be partially accounted for by considering a deviation of the current streamlines in the axial direction. The need of such deviation, which is also consistent with the presence of a finite electron Hall parameter, shows the intrinsic complexities of the axisymmetric configuration of MPD thrusters, which cannot be completely described in terms of the axial flow alone. Thus, in order to perform a fully two dimensional analysis of the problem and to preserve the essential character of the description, a magnetohydrodynamic approach[5] is considered as the object of further developments. Nonetheless, the parametric analysis and the simple approach proposed in the present paper give a clear description of the fundamental processes that characterize the plasma flow in MPD thrusters.

References

[1]Kuriki, K., Kunii, Y., and Shimizu, Y., "Idealized Model for Plasma Acceleration in an MHD Channel", *AIAA Journal*, Vol. 21, No. 3, 1981, pp. 322–326.

[2]Martinez-Sanchez, M., "Structure of Self-Field Accelerated Plasma Flows", *Journal of Propulsion and Power*, Vol. 7, No. 1, 1990, pp. 56–64.

[3]Fruchtman, A., "Limits on the efficiency of several electric thruster configurations", *Physics of Plasmas*, Vol. 10, No. 5, 2003, pp. 2100–2107.

[4]Maecker, H., "Plasma jets in arcs in a process of self-induced magnetic compression", *Zeitschrift für Physik*, Vol. 141(1), 1955, pp. 198–216.

[5]Andreussi, T., and Pegoraro, F., "Magnetized plasma flows and magnetoplasmadynamic thrusters", *Physics of Plasmas*, Vol. 17, No. 6, 2010, pp. 063507.